

# Interaction and mechanical effect of materials interface of contact zone composite samples: Uniaxial compression experimental and numerical studies

Wei qi Wang<sup>1,2</sup>, Yicheng Ye<sup>1,2,3</sup>, Qihu Wang<sup>\*1,2,3</sup>, Binyu Luo<sup>1,2</sup>, Jie Wang<sup>1,2</sup> and Yang Liu<sup>1,2</sup>

<sup>1</sup>School of Resources and Environmental Engineering, Wuhan University of Science and Technology, Wuhan 430-081, P.R. China

<sup>2</sup>Hubei Key Laboratory for Efficient Utilization and Agglomeration of Metallurgic Mineral Resources, Wuhan, 430-081, P.R. China

<sup>3</sup>Industrial Safety Engineering Technology Research Center of Hubei Province, Wuhan 430-081, P.R. China

(Received September 25, 2019, Revised May 12, 2020, Accepted May 18, 2020)

**Abstract.** Aiming at the mechanical and structural characteristics of the contact zone composite rock, the uniaxial compression tests and numerical studies were carried out. The interaction forms and formation mechanisms at the contact interfaces of different materials were analyzed to reveal the effect of interaction on the mechanical behavior of composite samples. The research demonstrated that there are three types of interactions between the two materials at the contact interface: constraint parallel to the interface, squeezing perpendicular to the interface, and shear stress on the interface. The interaction is mainly affected by the differences in Poisson's ratio and elastic modulus of the two materials, stronger interface adhesion, and larger interface inclination. The interaction weakens the strength and stiffness of the composite sample, and the magnitude of weakening is positively correlated with the degree of difference in the mechanical properties of the materials. The tensile-shear stress derived from the interaction results in the axial tensile fracture perpendicular to the interface and the interfacial shear fracture. Tensile cracks in stronger material will propagation into the weaker material through the bonded interface. The larger inclination angle of the interface enhances the effect of composite tensile/shear failure on the overall sample.

**Keywords:** contact zone composite sample; interface interaction; squeezing; derived stress; mechanical behavior

## 1. Introduction

There are a large number of composite rock masses composed of different components and structures in the earth's crust. Different lithology and structural characteristics make composite rock have significant anisotropy, which is the main factor leading to the instability and fracture of underground engineering (Klein *et al.* 2001, Müller *et al.* 2018, Zhang *et al.* 2018). The layered composite rock mass formed by sedimentation (Zhang *et al.* 2017, Xing *et al.* 2019, Zanjani and Soroush 2019) and the contact zone composite rock mass (Fig. 1) formed by magmatic intrusion and metamorphism (Machek *et al.* 2014, Ajalloeian *et al.* 2017, Cawood and Bond 2018) are two types of composite rock masses that are common in underground engineering.

A large number of studies on the mechanical behavior of layered composite rocks have been carried out. The results show that the differences in mechanical properties of different rocks have an important influence on the strength, deformation and failure mode of composite rock (Celleri *et al.* 2018, Alneasan *et al.* 2019, AlTammar *et al.* 2019, McBeck *et al.* 2019). The strength and elastic modulus of composite rock are lie between the different component materials, and the most deformable component governs the overall deformation of composite rock (Ferrill *et al.* 2012,



Fig. 1 Contact zone composite rock mass and composite rock sample

Amann *et al.* 2014, Chen *et al.* 2018). During compression, tensile cracks and shear cracks are generated in the strong and weak materials, respectively, forming a composite tensile-shear fracture (Liang *et al.* 2007, Li *et al.* 2014, Chen *et al.* 2019). The interaction between the two materials at the interface is the main cause of these results (Lu *et al.* 2017, Yue *et al.* 2018, AlTammar *et al.* 2019, Bauer *et al.* 2019, Yin *et al.* 2019). During deformation, different materials produce uncoordinated deformation at the contact interface, causing additional stresses in the strong material (tensile stress) and weak material (compressive stress) (Amann *et al.* 2011, Dubinya and Galybin 2018, Wang and Du 2019). With increasing confining pressure, the uncoordinated deformation weakens and the additional stress decreases, which in turn affects the mechanical characteristics of the composite sample,

\*Corresponding author, Professor, Ph.D.  
E-mail: wangqihu@wust.edu.cn

Table 1 Mechanical parameters of five kinds of material samples and corresponding material ratios

Sample number	Peak stress (MPa)	Axial strain at rupture (%)	Elastic modulus (GPa)	Poisson's ratio, $\mu$	Cohesion force (MPa)	Friction angle ( $^{\circ}$ )	Tensile strength (MPa)	Cement gypsum ratio	Sand plastic ratio	Water cement ratio
1	7.00	0.60	1.93	0.13	2.58	19.86	1.22	0.75	1.10	0.46
2	8.13	0.64	2.10	0.10	2.18	28.46	1.37	0.60	0.95	0.44
3	11.32	0.73	2.48	0.08	2.91	22.86	1.50	0.45	0.80	0.42
4	20.89	0.91	3.62	0.08	4.36	45.65	1.80	0.30	0.65	0.39
5	27.64	0.98	4.58	0.07	5.40	49.85	2.79	0.15	0.50	0.36

especially the expansion of the fracture (Liang *et al.* 2007, Li *et al.* 2014, Douma *et al.* 2019, Yang *et al.* 2019). Stronger interface bonding enhances uncoordinated deformation and composite fracture development.

At present, there are few studies on the mechanical behavior of the contact zone composite rock, mainly based on specific engineering cases. When the tunnel or chamber passes through the contact zone, there are obvious stress concentration and differentiations in the rock masses near the contact interface (Feng *et al.* 2012). Convergence differences between different rock masses are obvious, and shear fractures appear near the interface of composite rock masses (Panda *et al.* 2014; Xing *et al.* 2018). Different rock masses squeeze each other at the contact interface, resulting in a larger plastic zone in the weaker rock mass, accompanied by disasters such as roof falling (Yassaghi and Salari-Rad 2005, Feng *et al.* 2012).

There is obvious difference between the contact zone composite rock and the layered composite rock in component strength, degree of difference in mechanical properties of components, interface bonding strength and interface inclination angle. The strength of the contact zone composite rock is much larger than that of the layered composite rock (Yassaghi and Salari-Rad 2005, Liang *et al.* 2007), and the uniaxial compressive strength ratio of different component is about 1~2, while the layered composite rock is about 1~8 (Feng *et al.* 2012, Douma *et al.* 2019). There is strong adhesion between different components of the contact zone composite rock, rather than weak adhesion or friction, and the interface inclination angle is mainly within  $60^{\circ}$ ~ $90^{\circ}$  (Yassaghi and Salari-Rad 2005, Cawood and Bond 2018). Due to the large inclination of the interface, the interaction between different components of the contact zone composite rock exists in both the normal and tangential directions of the interface, while the interaction of the layered composite rock only exists in the tangential direction.

Based on the mechanical and structural characteristics stated above, it is necessary to carry out uniaxial compression test on the contact zone composite rock. The effect of the difference in mechanical properties of the components materials on the strength, deformation and failure of the contact zone composite rock are studied, the formation and influence mechanism of the interaction of different component in the direction parallel and perpendicular to the contact interface are analyzed, and discuss the formation and influence factors of shear stress at the interface, with the expectation to supply some basic information support for the stability study of contact zone

engineering. Due to the difficulty in sampling the contact zone composite rock, the test was carried out by preparing physically similar samples with an interface inclination of  $90^{\circ}$ . A numerical model of composite rock was constructed based on experiments to analyze the interaction perpendicular to the interface.

## 2. Experimental methodologies

### 2.1 Sample preparation

In order to ensure that the physical similar samples have good rock-like properties, P425 Portland cement, gypsum powder, river sand with particle diameters ranging from 0.9 to 1.2 mm and water were chosen as similar materials for preparing the samples (Hu *et al.* 2019, Huang *et al.* 2019). For more pronounced deformation and failure characteristics, the composite sample was designed to be a prism of  $100 \times 100 \times 200$  mm dimension. The ratios of five kinds of similar materials with different mechanical properties were determined by multiple adjustments and tests to simulate rocks with different mechanical properties. The ratios and mechanical parameters of five kinds of similar materials are listed in Table 1.

Two similar materials were separately filled on both sides of specially designed mold of  $100 \times 100 \times 200$  mm dimension, and the mold was fixed on vibration table, as shown in Fig. 2(a). The mold frame was divided into two parts 50 mm in width. A thin vertical plate was inserted between two parts. The similar materials were shaken for one minute after filled, and then pulled out the plate and shaking continued for one minute to compact the similar materials and bond the two materials.

By combining two different materials, ten sets of composite samples with different degrees of difference in mechanical properties of the two materials were obtained, and three samples were prepared for each group. The composite samples is identified using *a-b*. Where *a* and *b* correspond to the material numbers in Table 1. The elastic modulus ratio of the two materials was defined as  $\lambda = E_b/E_a$ , which was used to quantified the degree of difference in mechanical properties of the two materials of composite sample. Fig. 2(b) shown the prepared composite samples.

### 2.2 Experimental procedure

The testing system shown in Fig. 3 includes a loading module and deformation acquisition module. The loading system is YAW-1000A microcomputer controlled

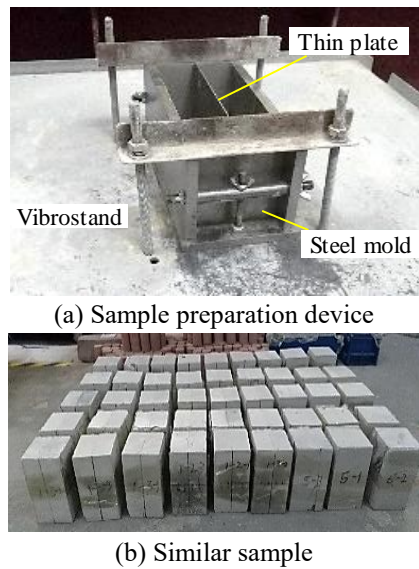


Fig. 2 Schematic diagram of sample preparation

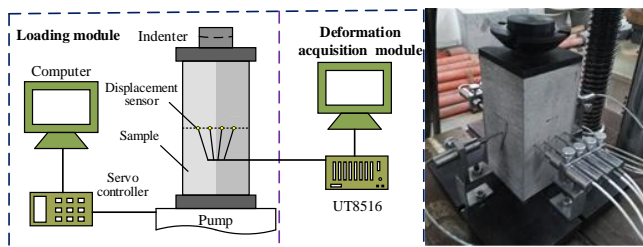


Fig. 3 Testing system schematic

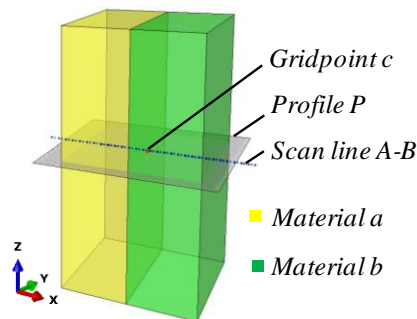


Fig. 4 Composite numerical model

electrohydraulic servo pressure machine, with maximum load of 1,000 kN. Testing samples were loaded at the loading rate of 0.002 mm/s. Two YWC-10 displacement sensors were installed on both sides of the contact interface in the middle of the composite sample. The distance between the sensors was 18 mm, monitoring the lateral deformation of the two materials parallel to the contact interface during loading. The displacement sensor has a monitoring range of 10 mm and an accuracy of 0.001 mm. UT8516 dynamic data acquisition instrument is adopted for deformation data acquisition, and the acquisition frequency is set to 25 Hz, the same as the press

### 2.3 Numerical model construction

The interaction between the two materials of the composite samples No. 1-5, No. 2-3, No. 3-4 and No. 3-5

Table 2 Mesoscopic parameters of single material model

Model number	Density (kg/m <sup>3</sup> )	Elastic modulus (GPa)	Poisson's ratio, $\mu$	Cohesion (MPa)	Friction angle (°)	Tensile strength (MPa)
1	2500	1.26	0.13	1.50	40	1.20
2	2500	1.27	0.10	1.80	40	1.60
3	2500	1.70	0.08	2.20	45	1.40
4	2500	2.36	0.08	3.40	50	2.00
5	2500	2.52	0.07	4.20	55	2.20

Table 3 Reduction factors of numerical model parameters

Model number	$R_E$	$R_c$	$R_t$
1-5	0.96	1.45	1.55
3-5	0.93	1.57	1.67
4-5	1.15	0.82	0.92

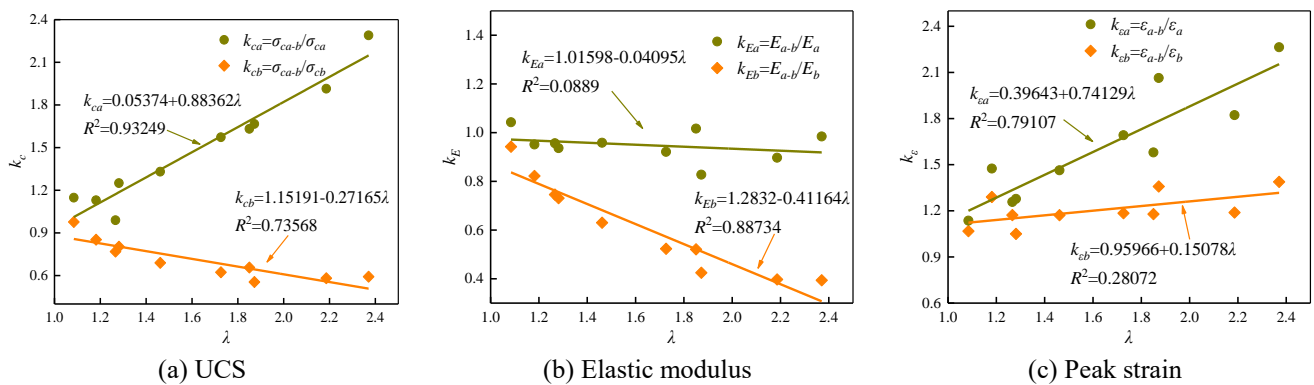
perpendicular to the contact interface was simulated. Numerical simulation is carried out using FLAC<sup>3D</sup> software, the numerical model of the composite sample has the same dimensions as the physically similar sample, and consists of 125,000 cells of  $2 \times 2 \times 4$  mm dimensions (Fig. 4). The model used strain softening constitutive model, based on the Mohr Coulomb failure criterion, the element only produces elastic strain at pre-peak stage, and produces elastic strain and plastic strain after yielding. The mesoscopic parameters of the model include bulk modulus, shear modulus, Poisson's ratio, cohesion, friction angle and tensile strength. The lower end surface has a zero displacement boundary, the upper end surface moves downward at a speed of  $2 \times 10^{-5}$  mm/step, and the side boundary is free. According to the stress-strain curve and mechanical parameters of the test (Table 1), the meso parameters corresponding to the five kinds of single material model were calibrated after multiple tests, as listed in Table 2.

The stress-strain curve, peak strain and uniaxial compressive strength (UCS) of the composite model were calibrated according to the test results. The calibration of the composite model parameters was achieved by reducing the mesoscopic parameters of the single material models and assigning them to different component materials of the composite model. The reduction is mainly due to the size effect between the composite model material and the single model material, and the interaction between the different materials. The reduction was achieved by multiplying the elastic modulus, cohesion and tensile strength of the two materials which constitute the composite model by the same reduction factor respectively and keeping the other parameters constant. The corresponding reduction factors of elastic modulus, cohesion and tensile strength are defined as  $R_E$ ,  $R_c$  and  $R_t$ , respectively. Based on the test results, after a series of tests, the reduction factors corresponding to the composite models No. 1-5, No. 2-3, No. 3-4 and No. 3-5 were determined, as listed in Table 3.

As shown in Fig. 4, a horizontal profile  $P$  is made in the middle of the composite model. Observe the stress and strain distribution of the two materials on the profile  $P$  in

Table 4 Uniaxial compression test results of composite samples

Sample number	Peak stress (MPa)	Elastic modulus (GPa)	Axial strain at rupture (%)	Modulus ratio, $\lambda$	Difference in Poisson's ratios, $\Delta\mu$
1-2	8.08	2.01	0.68	1.08	0.03
1-3	8.80	1.81	0.77	1.28	0.05
1-4	11.73	1.60	1.24	1.87	0.05
1-5	16.12	1.90	1.36	2.37	0.06
2-3	9.34	2.03	0.94	1.18	0.02
2-4	13.01	1.97	1.08	1.73	0.02
2-5	15.83	1.92	1.16	2.19	0.03
3-4	14.59	2.37	1.07	1.46	0.00
3-5	17.89	2.52	1.15	1.85	0.01
4-5	20.94	3.60	1.15	1.27	0.01

Fig. 5 The relationship between the ratio of mechanical parameters of composite sample to single sample and  $\lambda$ 

the horizontal and perpendicular to the contact interface direction ( $x$  direction). The scan line  $A-B$  is the midline in the  $x$  direction on the profile  $P$ . Record the stress ( $\sigma_x$ ) and strain ( $\varepsilon_x$ ) of the elements along the line  $A-B$  and the displacement of the gridpoint ( $c$ ) in the  $x$  direction to analyze the variation of the interaction during loading.

### 3. Analysis of uniaxial compression results

#### 3.1 The effect of $\lambda$ on mechanical parameters

The test results of the 10 sets of composite samples are listed in Table 4. The mechanical parameters of the composite sample and the single material sample (Table 1) were compared. The results shown that the strength of the composite samples is lie between the strength of the two components and closer to the higher material strength. The elastic modulus of the composite sample is almost always less than that of the two components and closer to the weaker material. The peak strain of the composite sample is greater than that of the two components. These result are different from the conclusion that the mechanical parameters of the layered composite rock are between the mechanical parameters of the two component materials (Liang *et al.* 2007, Chen *et al.* 2018).

Compared with the stronger components, the compressive strength of the composite sample is reduced and the deformability is increased. Comparing the

composite samples with different degree ( $\lambda$ ) of difference in mechanical properties of the two component materials, Fig. 5 shows that the difference in mechanical parameters between the composite sample and the single sample increases with an increase in  $\lambda$ . This indicates that the difference in mechanical properties of different materials leads to a weakening of the mechanical properties of the composite samples, and there is a positive correlation between them. The slope of the fitted curve in Fig. 5 indicates that the difference in mechanical properties of the different materials has a greater effect on the strength of the composite sample ( $k=0.8836$ ) than on the elastic modulus ( $k=0.4116$ ) and axial deformation ( $k=0.7412$ ).

#### 3.2 Typical stress-strain curves of uniaxial compression tests

As shown in Fig. 6, the stress-strain curves of the composite samples has good continuity. However, for the composite samples with a large difference in the mechanical properties of the two materials, the axial stress-strain curve has a turning phenomenon. The turning of the sample No. 2-5 ( $\lambda = 2.19$ ) with a larger  $\lambda$  value was more pronounced than that of the sample No. 1-4 ( $\lambda = 1.87$ ). Since the sample did not show macroscopic fracture when the curve turns, and the curve still shows a linear elastic increase after the turning, it can be inferred that the local damage at the contact interface inside the sample caused the curve to turn.

During the loading process, the lateral deformation

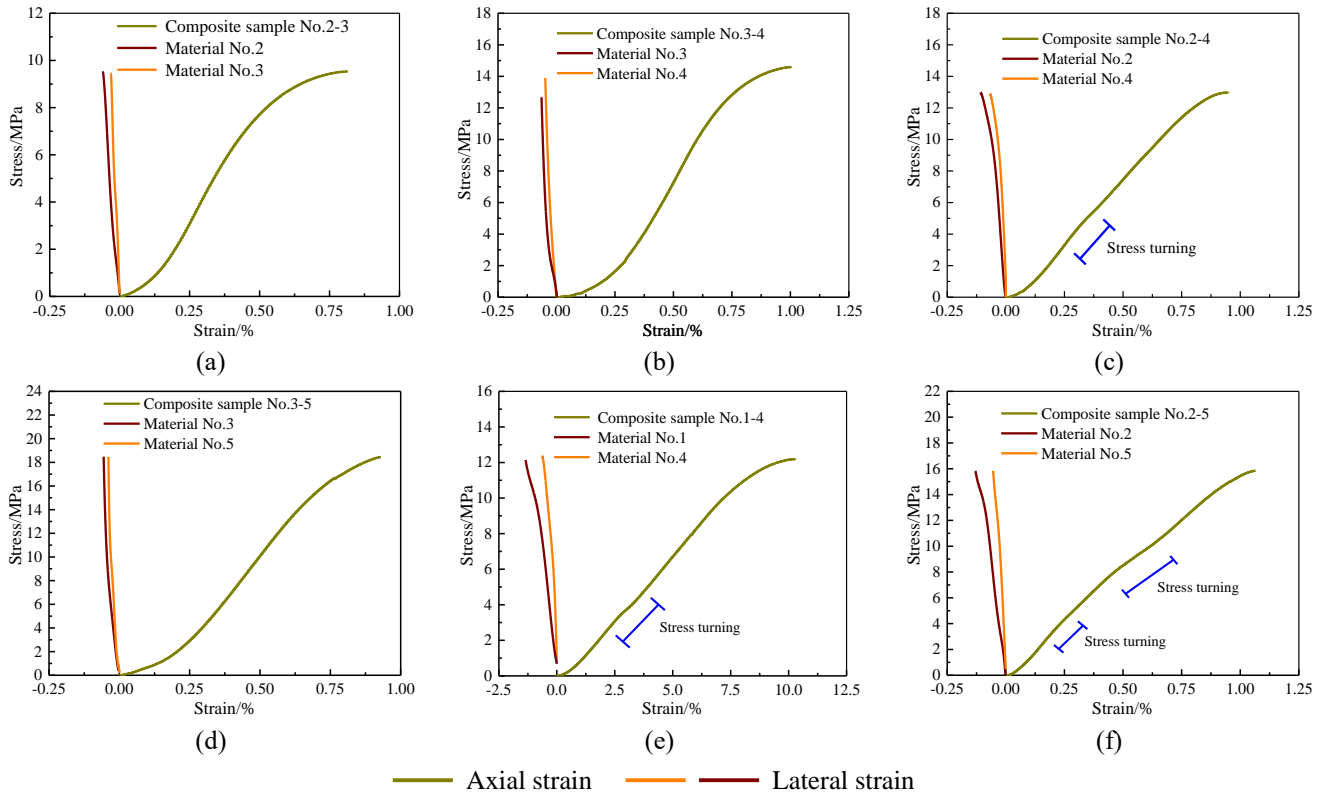


Fig. 6 Typical stress-strain curve of composite samples

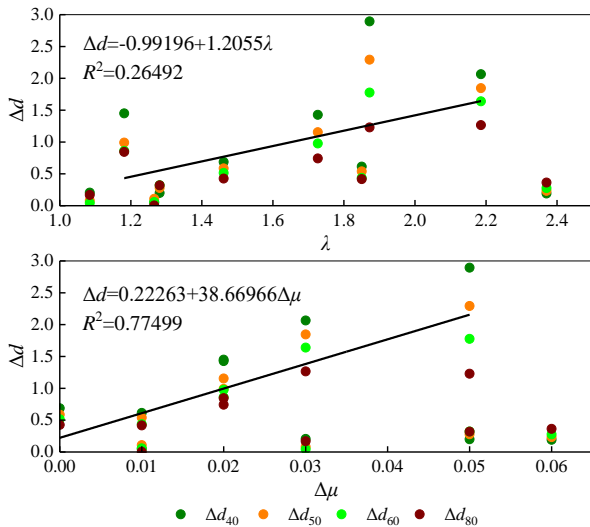


Fig. 7 The correlation of  $\Delta d$  with  $\lambda$  and  $\Delta\mu$ , respectively

parallel to the interface of the two materials on both sides of the interface is different, and is more obvious as the axial deformation increases. 40%, 50%, 60% and 80% of the strength of the composite sample were selected as four characteristic points. The ratio of the difference in lateral deformation of the strong material at the feature point is defined as  $\Delta d_{40}$ ,  $\Delta d_{50}$ ,  $\Delta d_{60}$ , and  $\Delta d_{80}$ , respectively. As shown in Fig. 7, in general, the degree of difference in the lateral deformation of the two materials of composite sample is positively correlated with the difference in their mechanical properties. Compared with the difference in elastic modulus

$\lambda$  ( $R^2=0.26492$ ), the degree of difference in the lateral deformation of the two materials is more correlated with the difference in Poisson's ratio  $\Delta\mu$  ( $\mu_a-\mu_b$ ) ( $R^2=0.77499$ ). The data processing method in Fig. 7 can eliminate the effects of deformation difference between different composite samples.

It can be concluded that, to some extent it is reasonable that the different lateral deformation of the two materials continuously transitions in some form near the contact interface before the contact interface is broken. The transition must be accompanied by complex interactions. Materials with large lateral deformation exert constrained tensile stress on materials with small lateral deformation, and materials with small lateral deformation are subjected to relative constrained compressive stress.

### 3.3 The effect of $\lambda$ on failure mode

Difference in failure modes of the composite samples was observed. In general, with the increase of the degree of difference in mechanical properties of the two materials, the failure modes of composite samples shows three types as follows.

(1) When the mechanical properties of the two materials are similar, a broken-line-typed shear fracture is formed mainly throughout the entire sample. The small axial fractures are formed near the contact interface, accompanied by slight tensile failure on the surface of the stronger material, as shown in Figs. 8(a) and 8(b).

(2) When the degree of difference in mechanical properties is greater, the shear fracture penetrates one or two materials. The contact interface occurs serious shear

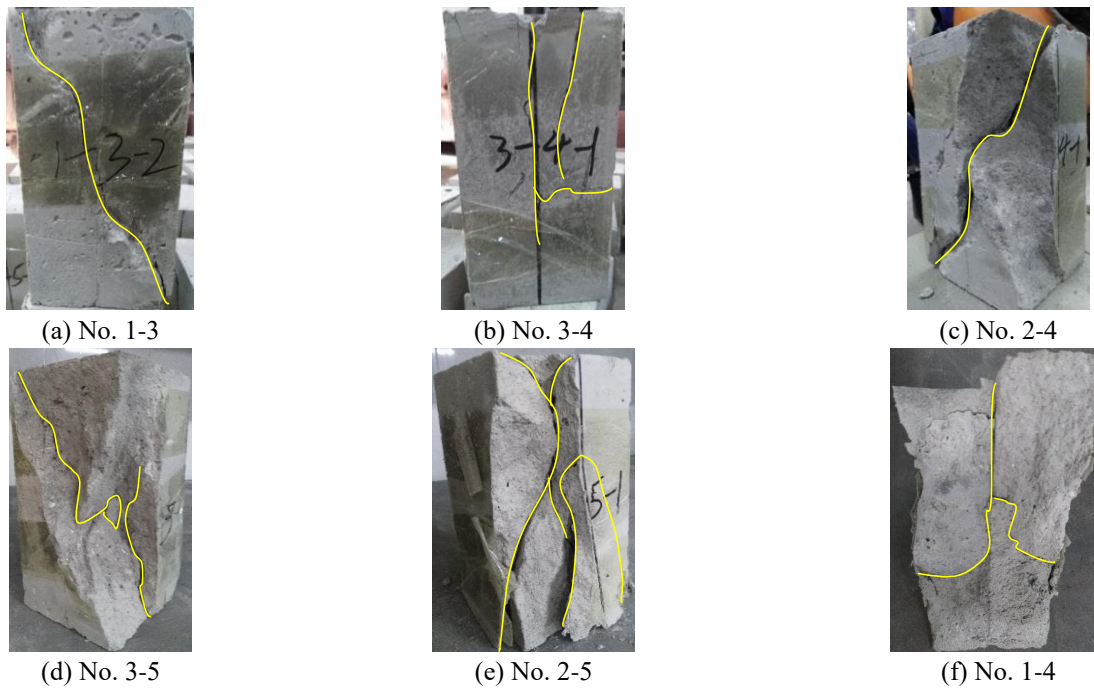


Fig. 8 Typical failure modes of composite samples

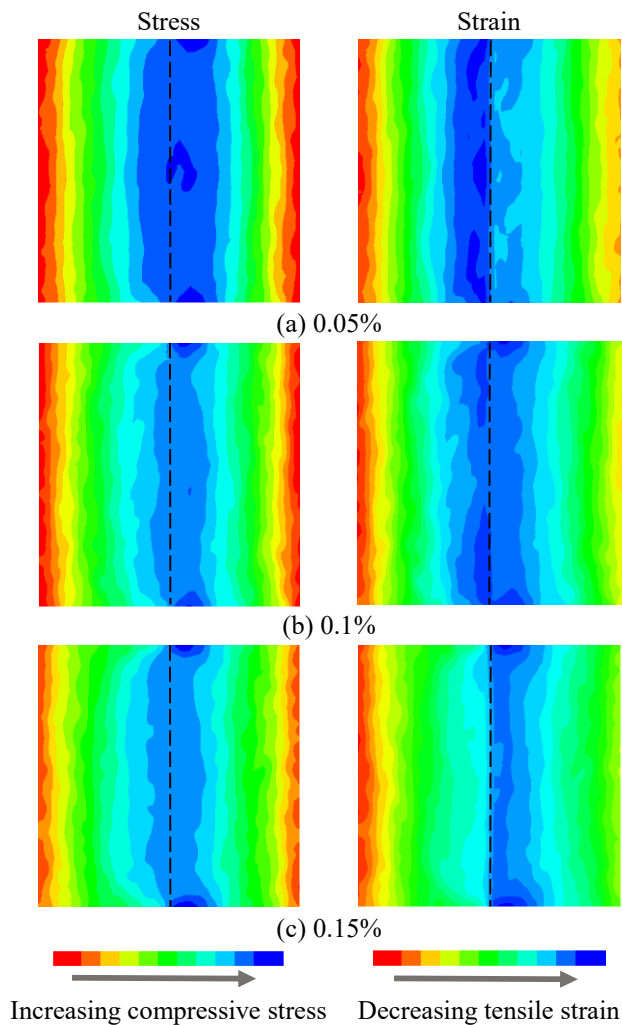


Fig. 9 The distribution of stress ( $\sigma_x$ ) and strain ( $\epsilon_x$ ) at different axial strain on the profile *P* of the model No. 3-5

failure, and the stronger material near the contact interface formed a tensile fracture perpendicular to the contact interface, as shown in Figs. 8(c) and 8(d).

(3) When the degree of difference is greater than 2.0, serious axial splitting failure occurs near the contact interface, and shear failure occurs on the weaker material side. The contact interface of sample No. 2-5 suffered shear failure, and the bonding almost completely failed. The shear and tensile fractures cut the sample into a plurality of blocks, and the main tensile fractures are perpendicular to the interface, as shown in Fig. 8(e).

Obviously, the difference in mechanical properties of the two materials leads to complex failure modes of the composite sample. These were attributed to the difference in lateral deformation of the two materials and the constraining effect produced by it. The distribution of tensile fractures indicates that its formation is affected by the constrained tensile stress. The formation and expansion of tensile fracture ultimately result in failure of stronger material. Under the interface bonding, the tensile fracture in the stronger material will propagation into the weaker material, as shown in Fig. 8(f). The shear failure of the interface show that the differential lateral deformation of different materials derives the shear stress on the contact interface, and the shear stress is positively correlated with the degree of difference in mechanical properties of the two materials.

There are obvious differences between the contact zone composite sample and the layered composite rock in the location and morphology of the failure. An axial tensile fracture perpendicular to the interface and an interfacial shear fracture were formed near the interface of the contact zone composite sample (Fig. 8). However, layered composite rocks such as coal rock and salt rock mainly form composite tensile-shear cracks that penetrate through the interface under compression. The tensile-shear cracks are mainly manifested as changes in the inclination angle,

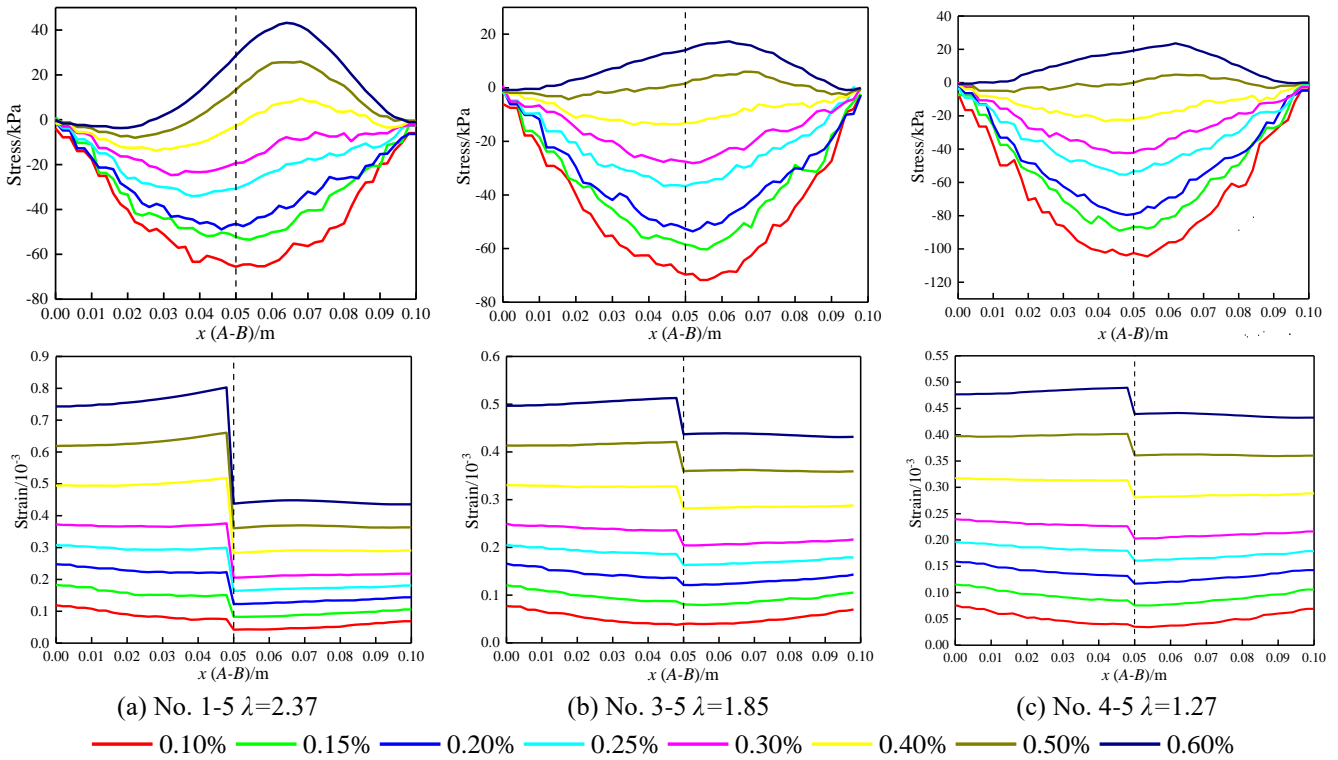


Fig. 10 The distribution of stress ( $\sigma_x$ ) and strain ( $\varepsilon_x$ ) of elements along scan line  $A-B$  under different axial strain

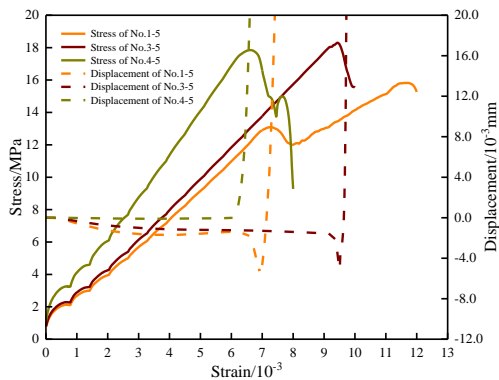


Fig. 11 Lateral displacement of gridpoint  $c$  perpendicular to the contact interface-axial strain of composite models

and the interface forms a slight local shear crack (Liang *et al.* 2007, Li *et al.* 2014). These directly lead to the difference in the extent and scope of damage between the two types of composite samples. Analysis shows that this can be attributed to the differences in the brittleness of the components and the bonding strength, inclination angle and dimension the interface of the two types of composite samples.

### 3.4 Stress and strain in perpendicular to contact surface

Fig. 9 shows the distribution of horizontal stress ( $\sigma_x$ ) and horizontal strain ( $\varepsilon_x$ ) perpendicular to the contact interface on the profile  $P$  of the composite model No. 3-5 during the initial phase of loading. The results show that the stress and strain of the two materials near the contact interface are significantly different. At 0.5% axial strain, the maximum

stress (compressive) is distributed on the side of the stronger material near the interface, and the tensile strain of the stronger material is greater than that of the weaker material. The difference in stress and strain between the two materials varies with the increase in axial strain.

The changes in horizontal stress ( $\sigma_x$ ) and horizontal strain ( $\varepsilon_x$ ) along scan line  $A-B$  during the test were observed. As shown in Fig. 10, there is stress and strain transfer between the two materials of the composite model. The maximum stress of the model gradually approaches the interface from the stronger material side, and the degree of the difference in stresses on both sides of the interface gradually decreases. The strain of stronger material near the interface experiences a change of smaller-equal-larger than that of weaker material. The transfer of strain precedes that of stress. The displacement of the gridpoint  $c$  in the  $x$  direction indicates that the stronger material near the interface displaced toward the weaker material side during the test, and the displacement tends to be stable with increasing axial strain before failure, as shown in Fig. 11.

Analysis shows that under axial compression, the two materials near the contact interface squeeze each other in the direction perpendicular to the interface, accompanied by changes of stress and strain between the materials. The squeezing is driven by the lateral unbalanced force between the two materials, which is strong at the beginning of the test and gradually decreases with the increase in axial strain, and finally tends to be stable. Comparing the composite models with different degrees ( $\lambda$ ) of difference in elastic modulus of the two materials in Figs. 10 and 11, it is found that the stress and strain of the model with larger  $\lambda$  have more significant differences on both sides of the interface. And the material with larger elastic modulus produced

greater displacement toward the side of the material with smaller elastic modulus, resulting in a more pronounced squeezing. These results indicate that the difference in elastic modulus of the two materials is the main influencing factor of the squeezing.

#### 4. Analysis of interaction mechanisms between different materials

##### 4.1 Squeezing in perpendicular to the contact interface

Materials with larger elastic modulus produce greater lateral compressive stress under axial compression. Therefore, the material near the contact interface is subjected to an unbalanced force toward the side of the material with smaller elastic modulus and is displaced to form a squeezing. This results in a decrease in the lateral strain of the material with smaller elastic modulus near the contact interface, and an increase in the lateral strain of the material with larger elastic modulus, which is manifested as the transfer of strain between the materials. According to Hooke's law, under a certain axial strain, the change of lateral strain will increase lateral stress of the material with small elastic modulus and reduce lateral stress of the material with large elastic modulus, which is manifested as the transfer of stress between the materials.

As shown in Fig. 12, the transfer of stress and strain in the material with smaller elastic modulus and the material with larger elastic modulus, respectively. Derived stress will further reduce the unbalanced force of the two materials near the interface. Therefore, the nature of the squeezing

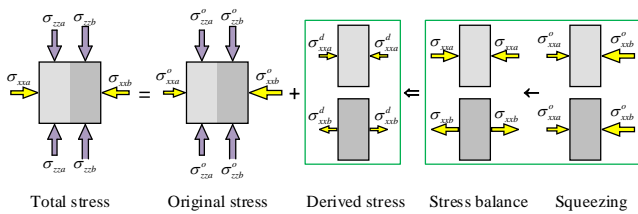


Fig. 12 The formation mechanism of squeezing and derived stress of two materials perpendicular to the contact interface.  $o$  and  $d$  denote the original stress and the derived stress, respectively; and  $\sigma_{xxa} = \sigma_{xxb}, \sigma_{xxa}^d = -\sigma_{xxb}^d$

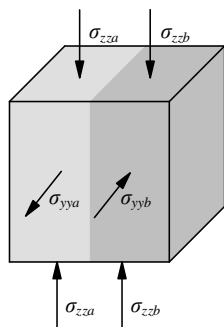


Fig. 13 Stress state of the composite unit near the contact interface

and the formation of the derived stress is the processes of stress balance. Due to the material with larger elastic modulus bear the main load during compression, therefore, the weakening of the mechanical properties of the stronger material by the derived tensile stress has a greater impact on the mechanical properties of the composite sample.

The two materials at the upper and lower ends of the contact zone composite rock are constrained by the roof-floor of the roadway or the indenter of the testing machine, which is the macro condition for squeezing. The end constraints restrict the lateral deformation of the material during loading. The two types of materials near the contact interface cannot expand outward freely, which in turn produces a squeezing perpendicular to the interface and transfers of stress and strain. The analysis shows that this is mainly caused by the large inclination angle of the contact interface of the contact zone composite rock ( $60^\circ$ - $90^\circ$ ), which proves that the structural difference between the contact zone composite rock and the layered composite rock has a significant effect on the interaction form near the interface.

##### 4.2 The constraint in parallel to the contact interface

Let  $E_a, E_b$  and  $\mu_a, \mu_b$  denote, respectively, the elastic modulus and Poisson's ratio and suppose  $E_a > E_b, \mu_a < \mu_b$ . Let  $\sigma_{zsa}, \sigma_{zsb}$  and  $\sigma_{yya}, \sigma_{yyb}$  are the axial stress and the constrained stress on the unit  $a$  and  $b$  near the interface, respectively, as shown in Fig. 13.

According to the static equilibrium condition and Hooke's law, the following stress-strain relationships of the composite unit should be satisfied:

$$\begin{cases} \sigma_{zz} = \frac{\sigma_{zsa} + \sigma_{zsb}}{2} \\ \sigma_{yya} = -\sigma_{yyb} \end{cases} \quad (1)$$

$$\begin{cases} \varepsilon_{zz} = \frac{\sigma_{zz}}{E_{zz}} \\ \varepsilon_{zsa} = \frac{1}{E_a}(\sigma_{zsa} - \mu_a \sigma_{yya}) \\ \varepsilon_{yya} = \frac{1}{E_a}(\sigma_{yya} - \mu_a \sigma_{zsa}) \\ \varepsilon_{zsb} = \frac{1}{E_b}(\sigma_{zsb} - \mu_b \sigma_{yyb}) \\ \varepsilon_{yyb} = \frac{1}{E_b}(\sigma_{yyb} - \mu_b \sigma_{zsb}) \end{cases} \quad (2)$$

where  $\sigma_{zz}, E_{zz}$  and  $\varepsilon_{zz}$  are the axial stress, elastic modulus and axial strain of the unit near the interface,  $\varepsilon_{zsa}, \varepsilon_{zsb}$  and  $\varepsilon_{yya}, \varepsilon_{yyb}$  are the axial and lateral strains of the two material units near the interface, respectively, which satisfy the following relationship at the contact surface:

$$\begin{cases} \varepsilon_{zz} = \varepsilon_{zsa} = \varepsilon_{zsb} \\ \varepsilon_{yya} = \varepsilon_{yyb} \end{cases} \quad (3)$$

The elastic modulus of the composite unit and the axial stress and lateral constrained stress of the two materials are

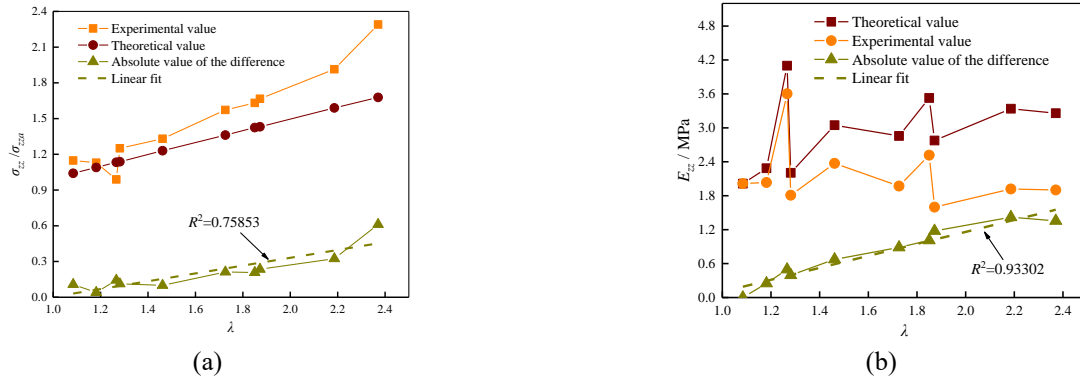


Fig. 14 Effects of  $\lambda$  on the experimental and theoretical values of (a)  $\sigma_{zz}/\sigma_{zza}$  and (b)  $E_{zz}$

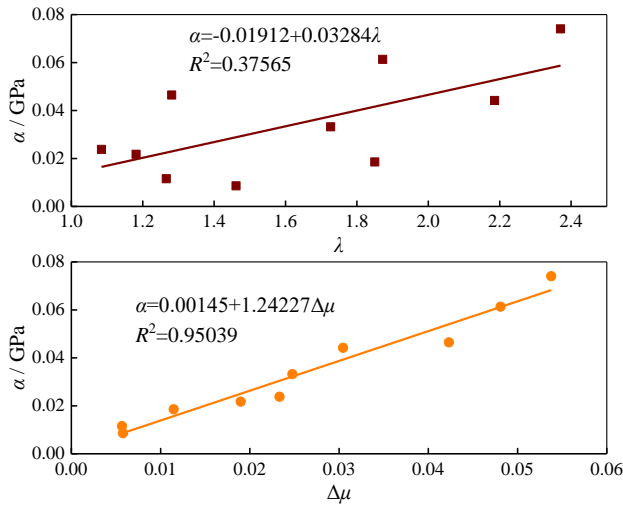


Fig. 15 The correlation of lateral constraint stress factor ( $\alpha$ ) with  $\lambda$  and  $\Delta\mu$

established respectively as follows by combination of Eqs. (1)-(3):

$$E_{zz} = \frac{E_a [(\lambda\mu_a + \mu_b)^2 - (\lambda + 1)^2]}{2[\lambda(\mu_a^2 - 1) + \mu_b^2 - 1]} \quad (4)$$

$$\begin{cases} \sigma_{zza} = \frac{E_a E_b (\mu_a \mu_b - 1) + E_a (\mu_b^2 - 1)}{E_a (\mu_b^2 - 1) + E_b (\mu_a^2 - 1)} \varepsilon_{zz} \\ \sigma_{zzb} = \frac{E_a E_b (\mu_a \mu_b - 1) + E_b (\mu_a^2 - 1)}{E_a (\mu_b^2 - 1) + E_b (\mu_a^2 - 1)} \varepsilon_{zz} \end{cases} \quad (5)$$

$$\sigma_{yya} = -\sigma_{yyb} = \frac{E_a E_b (\mu_b - \mu_a)}{E_a (\mu_b^2 - 1) + E_b (\mu_a^2 - 1)} \varepsilon_{zz} \quad (6)$$

Based on the test results in Fig. 5(a), the relationship between  $\sigma_{zz}/\sigma_{zza}$  and  $\lambda$  is analyzed by combination of Eqs. (2)-(5). Figure 14 shows that  $\sigma_{zz}/\sigma_{zza}$  has a strong correlation with  $\lambda$ , and the experimental values and theoretical values of  $\sigma_{zz}/\sigma_{zza}$  and  $E_{zz}$  with identical trend of variation. This shows that the theoretical model can well explain the effect of constraint on the strength and elastic modulus of the composite unit near the interface. However, as  $\lambda$  increases, the error between the theoretical and experimental values of

$\sigma_{zz}/\sigma_{zza}$  and  $E_{zz}$  increases regularly. The analysis shows that this phenomenon was attributed to the squeezing and shear stress at the contact interface, which proves from the side that there is a positive correlation between the degree of interaction and the degree of difference in mechanical properties of the two materials.

The coefficient of  $\varepsilon_{zz}$  in Eq. (6) is defined as the laterally constrained stress factor  $\alpha$ . Obviously,  $\alpha$  is a constant determined by the elastic modulus and Poisson's ratio of the two materials, and can be used to quantitatively analyze the constrained stress. Fig. 15 shows that the correlation between  $\alpha$  and  $\Delta\mu$  ( $R^2 = 0.90539$ ) is stronger than that between  $\alpha$  and  $\lambda$  ( $R^2 = 0.37655$ ), which is consistent with the experimental results reflected in Fig. 7.

Taking the composite sample No. 2-5 as an example, the relationship of  $\sigma_{yya}$  (0.04 MPa)  $= -\sigma_{yyb}$  (-0.04 MPa) in Eq. (6) proves that the constraint forms a constrained compressive stress (weak material) and a constrained tensile stress (strong material) in the two materials, changing the stress state of the materials. Fig. 15 shows that the value of  $\alpha$  is between 0.01 and 0.075, it can be speculated that after considering the squeezing and shear stress, the value of  $\alpha$  will further increase. The influence of interface interaction changes gradually near the contact interface, that is, there is a certain distance effect (Figs. 9 and 10). The interaction is strongest at the interface. On both sides of the interface, the interaction weakens with the increase of the distance from the interface, and the weakening in strong materials is more obvious and rapid. The weakening of interaction is a very complex phenomenon, which includes the variation of constraint parallel to the interface, squeezing perpendicular to the interface and shear stress on the interface. The theoretical model (Eqs. (1)-(6)) mainly explains the stress and strain of material elements with strong interaction near the interface, which provides a theoretical basis for revealing the interaction mechanism.

## 5. Discussion

The failure mode of the composite sample indicates that the differential deformation of different materials parallel to the contact interface result in shear stress near the contact interface, causing the shear failure of the interface shown in Fig. 8. Similar phenomena have been observed in layered

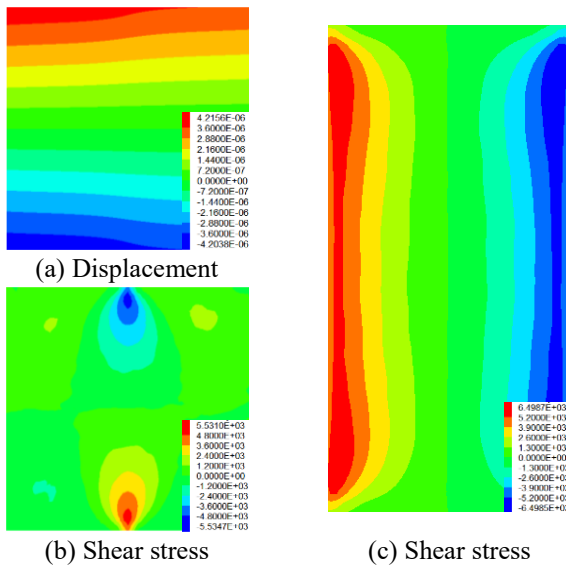


Fig. 16 The distribution of displacement ( $u_y$ ) and shear stress ( $\sigma_{xy}$ ) of the composite model No. 3-5 at 0.5% axial strain. (a) and (b) are the profile  $P$  and (c) is the contact interface

composite rock masses. However, there are different understandings of the formation mechanism and effects of shear stress.

The bond of the contact interface of the composite coal-rock mass is weak. Under the axial load, the radial relative deformation of coal and rock forms a frictional force at the interface, which is generally considered to be a constrained normal stress (Zhao *et al.* 2014). Liu *et al.* (2014) in the study of rock-coal-rock composites, considering the magnitude and influence range of the friction force gradually decreases from the interface to the end surface, and it has a conical distribution in the coal and rock body. The effect of interface constraints on the failure mode of the complex was well explained. For the salt rock with interlayer, there is no relative slip between the interlayer and the salt rock due to strong interface bonding. It is considered that the layered salt rock has shear stress caused by the interface cohesive component only near the interface of the inclined interlayer (Li *et al.* 2014). Further studies found that strain incompatibility exists near the interface of the salt rock interlayer resulted in many micro-shear cracks (Liang *et al.* 2007). However, even for composite salt rocks containing inclined interlayers, the interfacial shear failure does not occur under axial load.

Bourne (2003) first derived an analytical solution in three dimensions for the stresses of the interface-bonded composite layered rock under uniaxial loading normal to layering, indicating that in-plane tension develops in the stiffer layers and corresponding compression in the more compliant layers. Note that these in-plane stress contrasts are accompanied by the development of radial shear stress on the interfaces. For layered shale with strong layer bonding and brittle component, shear fracture parallel to the interface occurs under unconfined or slightly confined compressive loading normal to interface (Valrs *et al.* 2004, Niandou *et al.* 1997, Amann *et al.* 2011). These studies

show that the bonding state of the interface and the brittleness of the material have important effects on the shear stress and shear failure of the interface.

Under axial load, the two materials near the contact interface of the contact zone composite sample have different lateral deformations parallel to the interface, and the difference gradually increases from the interface center to the edges, as shown in Fig. 16. The magnitude of the shear stress corresponds to the degree of difference in later deformation, which is consistent with the test results of interface shear failure (Figs. 8(c)-8(e)).

The analysis shows that the interfacial shear failure of the contact zone composite sample is mainly affected by the differences in mechanical properties of two materials, the interface bonding state, and the components brittleness. Due to the stronger interface adhesion, the two materials with different lateral deformations maintain a coordinated meso-displacement near the contact surface, and the materials undergo relative displacement parallel to the interface, which in turn forms shear stress. The degree of relative displacement at the interface outside the sample is the largest, and gradually decreases toward the sides and center of the interface. Therefore, during the loading process, the shear stress at the interface edge first reaches the interface shear strength and shear failure occurs. In addition, the inclination angle of 60°-90° makes the influence range of the interface larger, resulting in more severe influence of the interface shear failure on the composite sample.

## 6. Conclusions

Based on the analysis of the test and numerical simulation, some conclusions have been made as follows:

- The differences in mechanical properties of different materials and the interaction near the interface significantly affect the strength, deformation and failure characteristics of the contact zone composite sample. The degree of influence is positively correlated with the degree of difference in the mechanical properties. The stronger component brittleness and interface adhesion and larger interface inclination angle make the interface interaction mode and failure mode of the contact zone composite rocks significantly different from those of the layered composite rocks.
- There is a constraint parallel to the interface and a squeezing perpendicular to the interface between the two materials near the contact interface, and are accompanied by a derived tensile-compressive stress. The differential lateral deformation of the two materials derives shear stress at the interface. Constraints and shear stress are mainly affected by differences in the Poisson's ratio of the materials and interface bonding strength. Squeezing is mainly affected by differences in the elastic modulus of the materials and interface inclination.
- Interaction at the interface lead to a complex failure mode of the composite sample. The derived tensile-shear stress forms an axial tensile fracture perpendicular to the contact interface near the interface, and s interfacial shear

fracture occurs, forming a composite tensile-shear failure. Affected by interface adhesion, tensile cracks in stronger materials will propagate into weaker materials. The larger interface inclination angle increases the influence range of interface failure.

- The expressions for the lateral constrained stress near the contact interface have been established. The existence of constrained tensile-compressive stress parallel to the interface was proved quantitatively, and the linear relationship between the constrained stress and the difference in Poisson's ratios of the two materials was determined combined with the experimental results.

## Acknowledgments

The authors acknowledge the financial support from the National Natural Science Foundation of China (Nos. 51704213 and 51574183), the Special Project of Central Government for Local Science and Technology Development of Hubei Province (2019ZYYD060) and the Open Fund of Hubei Key Laboratory for Efficient Utilization and Agglomeration of Metallurgic Mineral Resources in 2019 (No. 2019zy002).

## References

- Ajalloeian, R., Moghaddam, B. and Azimian, A. (2017), "Prediction of Rock Mass Squeezing of T4 Tunnel in Iran", *Geotech. Geol. Eng.*, **35**(2), 747-763. <https://doi.org/10.1007/S10706-016-0139-Y>.
- Alneasan, M., Behnia, M. and Bagherpour, R. (2019), "Analytical investigations of interface crack growth between two dissimilar rock layers under compression and tension", *Eng. Geol.*, **259**, 105188. <https://doi.org/10.1016/j.enggeo.2019.105188>.
- AlTammam, M.J., Agrawal, S. and Sharma, M.M. (2019), "Effect of geological layer properties on hydraulic-fracture initiation and propagation: an experimental study", *SPE J.*, **24**(2), 757-794. <https://doi.org/10.2118/184871-pa>.
- Amann, F., Button, E.A., Evans, K.F., Gischig, V.S. and Blümel, M. (2011), "Experimental study of the brittle behavior of clay shale in rapid unconfined compression", *Rock Mech. Rock Eng.*, **44**(4), 415-430. <https://doi.org/10.1007/s00603-011-0156-3>.
- Amann, F., Undul, O. and Kaiser, P.K. (2014), "Crack initiation and crack propagation in heterogeneous sulfate-rich clay rocks", *Rock Mech. Rock Eng.*, **47**(5), 1849-1865. <https://doi.org/10.1007/s00603-013-0495-3>.
- Bauer, S.J., Song, B. and Sanborn, B. (2019), "Dynamic compressive strength of rock salts", *Int. J. Rock Mech. Min. Sci.*, **113**, 112-120. <https://doi.org/10.1016/j.ijrmm.2018.11.004>.
- Bourne S.J. (2003), "Contrast of elastic properties between rock layers as a mechanism for the initiation and orientation of tensile failure under uniform remote compression", *J. Geophys. Res.*, **108**(B8), 1-11. <https://doi.org/10.1029/2001JB001725>.
- Cawood, A.J. and Bond, C.E. (2018), "3D mechanical stratigraphy of a deformed multi-layer: Linking sedimentary architecture and strain partitioning", *J. Struct. Geol.*, **106**, 54-69. <https://doi.org/10.1016/j.jsg.2017.11.011>.
- Celleri, H.M., Sánchez, M. and Otegui J.L. (2018), "Fracture behavior of transversely isotropic rocks with discrete weak interfaces", *Int. J. Numer. Anal. Meth. Geomech.*, **42**, 2161-2176. <https://doi.org/10.1002/nag.2849>.
- Chen, S.J., Yin, D.W., Jiang, N., Wang, F. and Guo, W.J. (2019), "Simulation study on effects of loading rate on uniaxial compression failure of composite rock-coal layer", *Geomech. Eng.*, **17**(4), 333-342. <https://doi.org/10.12989/gae.2019.17.4.333>.
- Chen, Y.L., Zuo, J.P., Liu, D.J. and Wang, Z.B. (2018), "Deformation failure characteristics of coal-rock combined body under uniaxial compression: Experimental and numerical investigations", *Bull. Eng. Geol. Environ.*, **78**(5), 3449-3464. <https://doi.org/10.1007/s10064-018-1336-0>.
- Douma, L.A.N.R., Regelink, J.A., Bertotti, G., Boersma, Q.D. and Barnhoorn, A. (2019), "The mechanical contrast between layers controls fracture containment in layered rocks", *J. Struct. Geol.*, **127**, 1-11. <https://doi.org/10.1016/j.jsg.2019.06.015>.
- Dubinya, N.V. and Galybin, A.N. (2018), "On Stress Distribution in Layered Rock Masses", *Izv. Phys. Solid Earth*, **54**(6), 904-913. <https://doi.org/10.1134/s1069351318060046>.
- Feng, W.K., Huang, R.Q. and Li, T.B. (2012), "Deformation analysis of a soft-hard rock contact zone surrounding a tunnel", *Tunn. Undergr. Sp. Technol.*, **32**, 190-197. <http://dx.doi.org/10.1016/j.tust.2012.06.011>.
- Ferrill, D.A., Morris, A.P. and McGinnis, R.N. (2012), "Extensional fault-propagation folding in mechanically layered rocks: the case against the frictional drag mechanism", *Tectonophysics*, **576**, 78-85. <https://doi.org/10.1016/j.tecto.2012.05.023>.
- Hu, B., Yang, S.Q., Xu, P. and Cheng, J.L. (2019), "Cyclic loading-unloading creep behavior of composite layered specimens", *Acta Geophys.*, **67**(2), 449-464. <https://doi.org/10.1007/s11600-019-00261-x>.
- Huang, C.C., Yang, W.D., Duan, K., Fang, L.D., Wang, L. and Bo, C.J. (2019), "Mechanical behaviors of the brittle rock-like specimens with multi-non-persistent joints under uniaxial compression", *Constr. Build. Mater.*, **220**, 426-443. <https://doi.org/10.1016/j.conbuildmat.2019.05.159>.
- Klein, E., Baud, P., Reuschlé, T. and Wong, T.F. (2001), "Mechanical behaviour and failure mode of Bentheim sandstone under triaxial compression", *Phys. Chem. Earth Solid Earth Geodes.*, **26**(1-2), 21-25. [https://doi.org/10.1016/S1464-1895\(01\)00017-5](https://doi.org/10.1016/S1464-1895(01)00017-5).
- Li, Y.P., Liu, W., Yang, C.H. and Daemen, J.J.K. (2014), "Experimental investigation of mechanical behavior of bedded rock salt containing inclined interlayer", *Int. J. Rock Mech. Min. Sci.*, **69**, 39-49. <http://doi.org/10.1016/j.ijrmm.2014.03.006>.
- Liang, W., Yang, C., Zhao, Y., Dusseault, M.B. and Liu, J. (2007), "Experimental investigation of mechanical properties of bedded salt rock", *Int. J. Rock Mech. Min. Sci.*, **44**(3), 400-411. <https://doi.org/10.1016/j.ijrmm.2006.09.007>.
- Liu, J., Wang, E.Y., Song, D.Z., Wang, S.H. and Niu, Y. (2014), "Effect of rock strength on failure mode and mechanical behavior of composite samples", *Arab. J. Geosci.*, **8**(7), 4527-4539. <https://doi.org/10.1007/s12517-014-1574-9>.
- Lu, S.Q., Li, L., Cheng, Y.P., Sa, Z.Y., Zhang, Y.L. and Yang, N. (2017), "Mechanical failure mechanisms and forms of normal and deformed coal combination containing gas: Model development and analysis", *Eng. Fail. Anal.*, **80**, 241-252. <http://doi.org/10.1016/j.engfailanal.2017.06.022>.
- Machek, M., Roxerová, Z., Závada, P., Silva, P.F., Henry, B., Dědeček, P., Petrovský, E. and Marques, F.O. (2014), "Intrusion of lamprophyre dyke and related deformation effects in the host rock salt: A case study from the Loulé diapir, Portugal", *Tectonophysics*, **629**, 165-178. <https://doi.org/10.1016/j.tecto.2014.04.030>.
- McBeck, J., Mair, K. and Renard, F. (2019), "Linking macroscopic failure with micromechanical processes in layered rocks: How layer orientation and roughness control macroscopic behavior", *Tectonophysics*, **750**, 229-242.

- <https://doi.org/10.1016/j.tecto.2018.11.016>.
- Müller, C., Frühwirth, T., Haase, D., Schlegel, R. and Konietzky, H. (2018), "Modeling deformation and damage of rock salt using the discrete element method", *Int. J. Rock Mech. Min. Sci.*, **103**, 230-241.  
<https://doi.org/10.1016/j.ijrmms.2018.01.022>.
- Niandou, H., Shao, J.F., Henry, J.P. and Fourmaintraux, D. (1997), "Laboratory investigation of the mechanical behavior of tournemire shale", *Int. J. Rock Mech. Min. Sci.*, **34**(1), 3-16.  
[https://doi.org/10.1016/S1365-1609\(97\)80029-9](https://doi.org/10.1016/S1365-1609(97)80029-9).
- Panda, M.K., Mohanty, S., Pingua, B.M.P. and Mishra, A.K. (2014), "Engineering geological and geotechnical investigations along the head race tunnel in Teesta Stage-III hydroelectric project, India", *Eng. Geol.*, **181**, 297-308.  
<http://doi.org/10.1016/j.enggeo.2014.08.022>.
- Valès, F., Minh, D.N., Gharbi, H. and Rejeb, A. (2004), "Experimental study of the influence of the degree of saturation on physical and mechanical properties in Tournemire shale (France)", *Appl. Clay Sci.*, **26**, 197-207.  
<https://doi.org/10.1016/j.clay.2003.12.032>.
- Wang, K. and Du, F. (2019), "Experimental investigation on mechanical behavior and permeability evolution in coal-rock combined body under unloading conditions", *Arab. J. Geosci.*, **12**(14), 1-15. <https://doi.org/10.1007/s12517-019-4582-y>.
- Xing, Y., Kulatilake, P.H.S.W. and Sandbak, L.A. (2018), "Effect of rock mass and discontinuity mechanical properties and delayed rock supporting on tunnel stability in an underground mine", *Eng. Geol.*, **238**, 62-75.  
<https://doi.org/10.1016/j.enggeo.2018.03.010>.
- Xing, Y., Kulatilake, P.H.S.W. and Sandbak, L.A. (2019), "Stability assessment and support design for underground tunnels located in complex geologies and subjected to engineering activities: Case study", *Int. J. Geomech.*, **19**(5), 1-9.  
[https://doi.org/10.1061/\(ASCE\)GM.1943-5622.0001402](https://doi.org/10.1061/(ASCE)GM.1943-5622.0001402).
- Yang, S.Q., Yin, P.F., Huang, Y.H. and Cheng, J.L. (2019), "Strength, deformability and X-ray micro-CT observations of transversely isotropic composite rock under different confining pressures", *Eng. Fract. Mech.*, **214**, 1-20.  
<https://doi.org/10.1016/j.engfracmech.2019.04.030>.
- Yassaghi, A. and Salari-Rad, H. (2005), "Squeezing rock conditions at an igneous contact zone in the Taloun tunnels, Tehran-Shomal freeway, Iran: a case study", *Int. J. Rock Mech. Min. Sci.*, **42**(1), 95-108.  
<https://doi.org/10.1016/j.ijrmms.2004.07.002>.
- Yin, D.W., Chen, S.J., Chen, B., Liub, X.Q. and Ma, H.F. (2018), "Strength and failure characteristics of the rock-coal combined body with single joint in coal", *Geomech. Eng.*, **15**(5), 1113-1124. <https://doi.org/10.12989/gae.2018.15.5.1113>.
- Yue, K., Olson, J.E. and Schultz, R.A. (2018), "Layered modulus effect on fracture modeling and height containment", *Proceedings of the Unconventional Resources Technology Conference*, Houston, Texas, U.S.A., July.
- Zanjani, M.M. and Soroush, A. (2019), "Numerical modelling of fault rupture propagation through layered sands", *Eur. J. Environ. Civ. Eng.*, **23**(9), 1139-1155.  
<https://doi.org/10.1080/19648189.2017.1344148>.
- Zhang, G.H., Jiao, Y.Y., Ma, C.X., Wang, H., Chen, L.B. and Tang, Z.C. (2018), "Alteration characteristics of granite contact zone and treatment measures for inrush hazards during tunnel construction – A case study", *Eng. Geol.*, **235**, 64-80.  
<https://doi.org/10.1016/j.enggeo.2018.01.022>.
- Zhang, N., Shi, X.L., Wang, T.T., Yang, C.H., Liu, W., Ma, H.L. and Daemen, J.J.K. (2017), "Stability and availability evaluation of underground strategic petroleum reserve (SPR) caverns in bedded rock salt of Jintan, China", *Energy*, **134**, 504-514. <http://doi.org/10.1016/j.energy.2017.06.073>.
- Zhao, Z.h., Wang, W.M., Dai, C.Q. and Yan, J.X. (2014), "Failure characteristics of three-body model composed of rock and coal with different strength and stiffness", *Trans. Nonferr. Met. Soc.*, **24**(5), 1538-1546.  
[https://doi.org/10.1016/S1003-6326\(14\)63223-4](https://doi.org/10.1016/S1003-6326(14)63223-4).

CC